Turkish Journal of Chemistry

http://journals.tubitak.gov.tr/chem/

Research Article

Turk J Chem
(2014) 38: 686 – 700

doi:10.3906/kim-1311-6

Linear assembly and 3D networks of peptide modified gold nanoparticles

Şaban KALAY[1], Clement BLANCHET[2], Mustafa CULHA[1,*]
[1]Department of Genetics and Bioengineering, Yeditepe University, Ataşehir, İstanbul, Turkey
[2]EMBL Hamburg, Hamburg, Germany

Received: 05.11.2013 • **Accepted:** 12.03.2014 • **Published Online:** 15.08.2014 • **Printed:** 12.09.2014

Abstract: The charge and size of molecules chemically attached to nanoparticles (NPs) play an important role in their interaction behavior in suspensions. Gold nanoparticles (AuNPs) were modified systematically with peptides and the modification was verified with surface-enhanced Raman scattering (SERS). The behavior of the modified AuNPs in suspension and at the liquid–solid interface was monitored using small angle X-ray scattering (SAXS), UV/Vis spectroscopy and dynamic light scattering (DLS) in suspension, and atomic force microscopy (AFM) at the solid–liquid interface. It was found that while negatively charged peptide modified AuNPs behave very similar to citrate reduced AuNPs due to their negatively charged surface, positively charged peptide modified AuNPs showed significantly different assembly/aggregation properties in suspension. The formation of linear assemblies of positively charged peptide (CKRHSKRHRSKRHSKRHSKRHSKR) modified AuNPs was clearly observed from the AFM analysis of the droplet areas of its colloidal suspension. The combined analyses of data obtained from the employed techniques suggest that the positively charged large peptide modified AuNPs can form linear and 3D-like networks in the suspension. This study reveals important information regarding the surface property dependent behavior of NPs that may help in efforts to build higher structures using NPs as building blocks.

Key words: Gold nanoparticles, self-assembly, charged peptides, atomic force microscopy

1. Introduction

The ability to control the construction of higher order nanostructures using nanoparticles (NPs) as building blocks is one of the biggest dreams of nanotechnologists. In order to achieve this goal, several approaches have been reported recently.[1–3] However, the challenge to control the behavior of the NPs in suspensions and at interfaces remains intact. Self-assembly refers to the self-organization of the components to form higher ordered structures without any outside intervention.[4] The inspiration of building higher order structures from NPs comes from the astonishingly powerful molecular self-assembly process that the process of living relies on. Therefore, the use of biological macromolecules for NP assembly is increasingly attracting attention. The self-assembly of biomolecule modified AuNPs and AgNPs has been extensively studied.[5,6] Biomolecules such as nucleic acids,[7] peptides,[8] lipids,[9] and carbohydrates[10] are used for the NP modification and self-assembly process. The main reason behind the use of biomolecule-modified NPs is to benefit from the existing weak forces among the biomolecules such as van der Waals, hydrogen bonds, dipole–dipole, and ionic interactions to control the assembly process.

Peptides are the most commonly employed group of biological macromolecules in NP modification due

*Correspondence: mculha@yeditepe.edu.tr

to their easy design and synthesis, and thus easy manipulation of their charge status and polarity.[11,12] The rationale behind their use is the utility of the weak interactions pertaining to side residues, which governs the self-assembly process. Peptides have been used for constructing ordered structures through their self-assembly. Best known are the nanotubes formed from Phe–Phe found in β-amyloids.[13,14] With the preparation of amino acid modified NPs, the assembly of peptide modified NPs has been investigated.[15−19] Bishnoi et al. showed that some specific sequences of the peptides can bind to AuNPs and the assembly and aggregation parameters can be adjusted by varying pH.[16] Levy and his group performed several studies about peptide capping ligands for NPs.[17] However, after the peptide modification, it was observed that the NPs in the suspension were unstable and precipitated quickly. The stability of the NPs is directly related to the charge double layer on the NP surfaces. Previous studies indicate that AuNPs capped with negatively charged peptides show higher stability than AuNPs capped with positively charged peptides.[16] A study reported by Levy's group demonstrated that a special sequence CALNN showed great stability, and they also indicated that cationic peptide modified AuNPs were not stable.[17] Krpetic et al. synthesized some specific peptides and investigated the behavior of peptide modified AuNPs on hydrophilic surfaces.[19] They used cysteine and lysine containing peptides as capping agents in the preparation of monolayer protected AuNPs. A study done by Chen and his group showed that by using peptides the NPs can be assembled as a nanoribbon.[18] They used peptides with the amino acid sequence AYSSGAPPMPPF. Furthermore, the latest study showed that modified AuNPs could enable the in vivo detection of tumors several millimeters in size.[20]

According to the Derjaguin–Landau–Verwey–Overbeek (DLVO) theory, the stability of NPs in a suspension depends on the surface charge, which bears the repulsion forces and the van der Waals attraction forces between the NPs.[21] Surface charges of NPs cause the formation of a double layer on the NP surface, called counterions, which causes a repulsive force against the van der Waals attraction forces. This prevents NP aggregation and stabilizes the colloidal solution. It was found that the stabilization of NPs with peptides can only be achieved by using negatively charged peptides and also it was found that when cationic peptides were used the cationic groups of the peptides interacted with the citrate ions and caused a bridging effect that led to NP aggregation.[19] A study by Lin et al. showed that cationic or neutral molecule addition could be done by a 2-step method.[22] They first replaced citrate with another molecule like thioctic acid and then the desired neutral or cationic exchanged with the thioctic acid. Serizawa and his group showed a technique for one-step peptide modification on NPs. They used HEPES as the reducing agent.[23]

Small-angle X-ray scattering (SAXS) is a powerful tool to study the structure of various systems at a resolution from about 1 to 100 nm.[24] SAXS data analysis allows one to build a low-resolution 3D model of different samples. In particular, an ab initio method for low-resolution shape reconstruction, along with rigid body modeling methods, although originally developed for protein can be employed to analyze other samples and to build structural models of complex natural or artificial materials.[25]

The interactions of AuNPs with BSA[26] or HSA[27] rather than a peptide were investigated in recent studies. There is no study that shows the interaction of AuNPs with systematically designed positively and negatively charged peptides in the literature. In this study, we investigated for the first time the stability and the self-assembly behavior of anionic and cationic peptide modified AuNPs in suspension and at the liquid–solid interface. For this, custom designed positively and negatively charged peptides were used. Peptides can bind to the surface of AuNPs through their thiol groups, which are found at the N-terminal cysteine of all peptides. The peptide binding was characterized by SERS. Using UV/Vis spectroscopy and dynamic light scattering (DLS) the anionic and cationic peptide binding properties were investigated. We characterized the NPs and

their aggregation states using SAXS, through which we constructed a 3D model of the networks of NPs. These structures were also directly imaged using atomic force microscopy (AFM). We also investigated the shape of peptide coated AuNPs by building an ab initio dummy atom model from the SAXS data. A detailed study of the aqueous phase, 3-dimensional structure of the peptide-linked NP assemblies was conducted.

2. Results and discussion

2.1. Characterization of peptide modified AuNPs

The use of peptides for modification has the advantage of systematic surface property alterations of AuNPs for a number of applications such as self-assembly.[6,11,12] The hydrophobicity can be easily tuned by changing the composition of the peptide sequence. In this study, gold binding peptides were designed to bind and coat the AuNP surfaces. The amino acid sequences, codes, net charge at the studied pH, and some physicochemical properties of the designed peptides are provided in Table 1. The positively charged peptides contain lysine, arginine, and histidine as positively charged amino acids. The negatively charged peptides contain aspartic acid and glutamic acid as negatively charged amino acids. All peptides exhibit a very hydrophilic character and are highly soluble in water. Since the functional groups such as –SH and charged side chain strongly interact with the AuNP surface,[28−30] all peptides were designed to have a cysteine residue at the N terminus to increase the binding stability. The charge on each peptide is gradually increased for both anionic and cationic sequences. Among the anionic peptides, P1 possesses 2 acidic ionizable –COOH groups, while P5, P16, P18, and P20 possess 4, 9, 10, and 11 ionizable –COOH groups, respectively. The net charges of these peptides range from –1.0 to –9.8. For the cationic peptides, 3 basic amino acids are systematically included in the structure. While P2 possesses 3 basic ionizable $–NH_2$ groups, P6, P10, P14, P17, P19, P21, and P23 possess 4, 6, 8, 9, 10, 12, and 13 ionizable $–NH_2$ groups, respectively. P23 also contains a small α-helix as underlined in Table 1. The net charges of the cationic peptides range from +2.0 to +16.8.

Table 1. Structure and some physicochemical properties of peptides used*.

Code	Sequence	Resid. numb.	Estimat. charg. pH 6	Iso - elec. point, pI	MW (g/mol)	Hydrophilic. resid. / Total resid. (%)
P1	CSE	3	–1.0	3.3	337.4	67%
P2	CKR	3	+2.0	10.1	405.5	67%
P5	CSEDSD	6	–2.9	2.9	654.6	83%
P6	CKRHSK	6	+3.7	10.6	757.9	67%
P10	CKRHSKRHR	9	+6.5	12.1	1207.4	67%
P14	CKRHSKRHRSKR	12	+8.5	12.4	1578.9	75%
P16	CSEDSDESDSESDSE	15	–7.8	2.6	1620.4	93%
P17	CKRHSKRHRSKRHSK	15	+10.3	12.4	1931.3	73%
P18	CCSEDSDESDSESDSESDS	19	–8.8	2.6	2012.8	89%
P19	CKRHSKRHRSKRHSKRHS	18	+12.0	12.6	2311.7	72%
P20	CCSEDSDESDSESDSESDSES	21	–9.8	2.6	2229.0	90%
P21	CKRHSKRHRSKRHSKRHSKRH	21	+14.8	12.7	2733.2	71%
P23	CKRHS<u>KRH</u>RSKRHSKRHSKRHSKR	24	+16.8	12.8	3104.6	75%

*The estimated charge, pI, MW, hydrophilic residue ratio of peptides can be calculated based on an input sequence by an online program available at the Innovagen web site. The secondary structure can be predicted by using a program Jpred available from the ExPASy web site.

Surface-enhanced Raman spectroscopy (SERS) was used for the verification of the peptide attachment to the AuNP or AgNP surfaces.[16,17,21,22] The use of this technique to prove that the peptides were attached to AuNPs was reported.[31] However, the reported results indicate that there is not a general consensus about the bands confirming the presence of the peptide on the Au surface.

Perhaps this results from the difficulty in obtaining a healthy SERS spectrum due to the fact that a number of parameters such as aggregation status of NPs and laser wavelength can influence a SERS experiment. Figure 1 shows the SERS spectra of citrate capped AuNPs and negatively and positively charged peptide attached AuNPs.

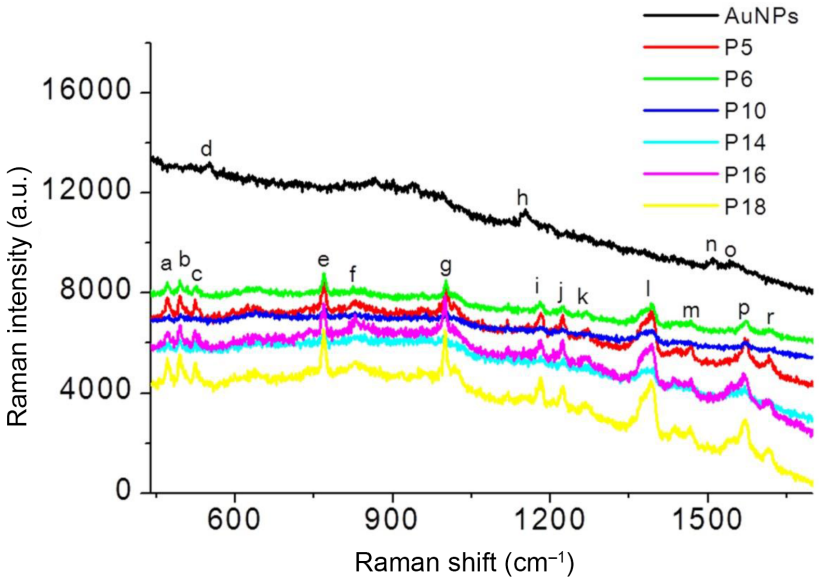

Figure 1. SERS spectra of unmodified and peptide modified AuNPs. a) 468 cm^{-1}, b) 492 cm^{-1}, c) 521 cm^{-1}, d) 548 cm^{-1}, e) 765 cm^{-1} histidine amino acids,[33] f) 829 cm^{-1}, C–S–C stretching band (819 cm^{-1}), g) 999 cm^{-1} C–C stretching, h) 1150 cm^{-1} C–N protein assignment, i) 1181 cm^{-1}, j) 1220 cm^{-1} amide III (arising from coupling of C–N stretching and N–H bonding; can be mixed with vibration of side chains),[34,35] k) 1272 cm^{-1} amide III (1230–1300 cm^{-1}), l) 1392 cm^{-1}, m) 1446 cm^{-1} CH_2 scissoring, CH_2 bending modes,[34] n) 1509 cm^{-1}, o) 1527 cm^{-1}, p) 1567 cm^{-1}, r) 1615 cm^{-1}, associated with the vibrations of the amide I.[32,34]

From the SERS spectra, it can be easily seen that there are spectral differences between the modified and unmodified AuNPs. The intensities of the bands in the SERS spectra differ from peptide to peptide (Figure 1). The peak intensities of the shortest and the longest ionic peptide modified AuNPs are low when compared to the others. This could be due to the high density packing of short peptide modified AuNPs, which has a negative effect on SERS enhancement. In the long peptide conjugated AuNP case, it could be due to the lower number of peptides binding to the AuNP surface due to the large size of peptides. Here for cationic peptide modified AuNPs it can also easily be seen that the intensities of the bands are very low when compared to the anionic peptide modified AuNPs. Moreover, the intensities decrease with the increasing size of the peptide. Thus, it can be concluded that there are fewer peptides in close proximity to the NP surfaces. On the SERS spectra, the bands at around 1615 cm^{-1}, 1547 cm^{-1}, 1571 cm^{-1}, and 1272 cm^{-1} may be associated with the peptide backbone. The band at around 1615 cm^{-1} is associated with the vibrations of the amide I.[32]

The strong band at around 999 cm^{-1} is attributed to –C–COO^- stretching. The band at 765 cm^{-1} originates from the vibrational modes of –COO^- terminal groups. The bands at 1571 cm^{-1} and 1392 cm^{-1} indicate the asymmetric and symmetric stretching modes of the –COO^- group, respectively. These results are in good agreement with the previously reported data.[33–37]

2.2. Behavior of peptide modified AuNPs in suspension

The binding of peptides on NPs was aimed through the –SH in the N-terminal of the peptide sequence as stated above. First, change in the starting concentration of the negatively charged peptides added to the AuNP suspension caused a few observable differences, while positively charged peptides resulted in some aggregate formation. The number of peptides per AuNP was decreased to about 200, which generated a stable colloidal suspension. The number of peptide molecules per AuNP was approximately calculated by considering the theoretical size of peptide from the contact point (thiol group possessing end) to the AuNPs, AuNP surface area, and the estimated concentration of the AuNPs in the suspension.[38,39] It should be noted that there was no adjustment to the pH of the colloidal suspension. The pH before and after the addition of the peptides was in the range of 5.9–6.0. It should be noted that at this pH all the peptides are in their ionized form. Figures 2A–2D show the DLS spectra and color change of AuNP suspensions with the addition of all charged peptides. According to our DLS results, size distribution area was gradually narrowed by modification of the anionic peptides and the intensity of the size distribution curve was slightly changed (Figure 2A). This may indicate that a more monodisperse structure occurred with the anionic peptide modified AuNPs rather than AuNPs. The UV/Vis spectroscopic evaluation of AuNP colloidal suspension indicated that the AuNPs modified with negatively charged peptides were very stable and well dispersed in suspension. A slight change in their surface plasmon resonance (SPR)[40] band as the negatively charged peptides were added into the AuNP colloidal

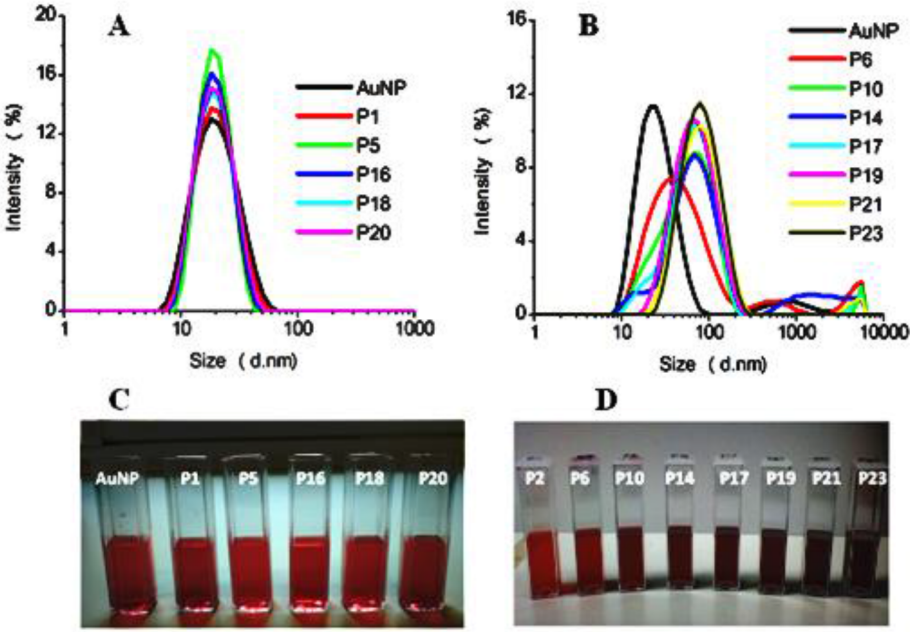

Figure 2. DLS spectra and color change of AuNP suspensions after addition of negatively charged (A and C) and positively charged (B and D) peptides.

suspension was observed. With the addition of each anionic peptide, there was a slight change in the size and surface charge of the AuNPs in suspension (data not shown). The AuNPs were modified with positively charged peptides and an increase in the size of the AuNPs in the suspension (Figure 2B) due to aggregate formation was observed from DLS measurements while no significant difference in the zeta potentials was observed. The zeta potential measurement with DSL is based on the assumption that the particles are spherical. The failure of the surface zeta potential measurement indicates that the aggregates are not spherical and, as mentioned earlier, this is another indication that AuNPs modified with positively charged peptides form networks in the suspension. Due to this fact, the surface charge cannot accurately be measured to the positively charged peptide.

A small red shift was observed with the addition of the largest peptide. For example, the SPR of pure AuNPs was measured as 520 nm and this value shifted to 523 nm as P23–AuNPs bound to the AuNP surface. There was no precipitation as anticipated and the formed peptide AuNPs structure was remarkably stable. The anionic peptide size increased systematically; the AuNPs–peptide conjugate size also increased, but not systematically. No color changes were observed with the addition of the anionic peptides (Figure 2C). In the case of the cationic peptides, the color of the AuNP suspension gradually changed from ruby red color to dark blue depending on the cationic peptide size (Figure 2D).

2.3. Peptide-binding study

The molar extinction coefficient value of the AuNPs changes depending of the size of AuNPs.[41,42] The quality of the water, magnetic stir bars, and clean equipment used in the synthesis of the AuNPs influence their synthesis. All equipment to be used for this purpose is recommended to be cleaned with HCl/HNO_3 (3:1 v/v).[42] The molar extinction coefficient value of 3–40 nm size can be determined using the equation[41] $\ln \varepsilon = k \ln D + a$. In this equation, ε is the extinction coefficient, in $M^{-1}\ cm^{-1}$; D is the core diameter of the nanoparticles; and k = 3.32111, a = 10.80505. The initial concentration of the AuNPs of the P23 binding study was calculated to be 2.46 nM by this equation.

The titration of AuNP suspension may provide valuable information about the binding properties of peptide to the surface of AuNPs. For the study of binding properties the AuNP suspension was titrated against P2, P5, P23, and water (control). The titration curves of the negatively and positively charged peptides with AuNPs are presented in Figures 3A–3D. The SPR band intensity increased slightly with increasing concentration of P5; during this process, there was almost no shift in the position of the SPR band. The increase in the intensity of the SPR band continued until the peptide concentration reached a certain level. After this point, a decrease in the intensity of the SPR was observed due to the possible dilution effect (Figure 3A indicated by red arrow). A small red shift ($\sim$2 nm) was also observed during the P5 titration. Tullman et al. also observed a similar profile with the negatively charged biotin-AHAHAHA peptide and explained that absorbance increase by a change in the local dielectric permittivity upon peptide binding or the stabilization of the AuNPs in buffer solutions.[16] On addition of positively charged peptides to the AuNP suspension a broad band in the range of 600 to 700 nm emerged with the increasing size and charge of the added peptides while the maximum absorption band gradually decreased in intensity, as seen in Figures 3B and 3C. The results indicated that there was a direct relationship between cationic peptide size and forming aggregate size. As the peptide size increased, the aggregate size increased.

The interaction of AuNPs with (+) charged peptides was investigated in P2 and P23 titration studies. P2 is a relatively small peptide sequenced CKR, and P23 is a relatively big peptide sequenced CK-RHSKRHRSKRHSKRHSKRHSKR. The SPR band intensity decreased with the addition of P2, resulting in a

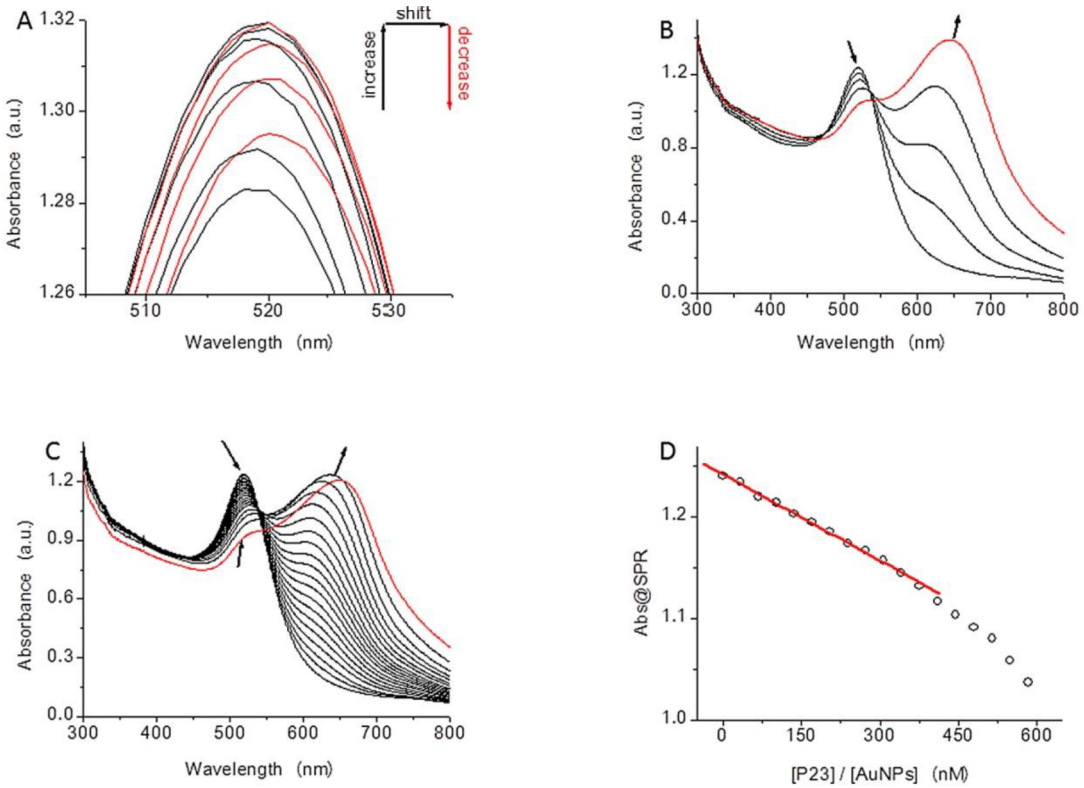

Figure 3. Titration spectra of the AuNPs suspensions against negatively and positively charged peptides. Increase and decrease in intensity of SPR band with increasing P5 concentration (A). Change in SPR band as positively charged P2 and P23 concentrations increase (B and C, respectively). Binding curve of P23 to colloidal AuNPs (D). The end point of the titration experiments are indicated by a red line (B and C).

small red shift (2 nm), and at the same time an aggregation peak at around 650 nm is seen (Figure 3B). A similar observation was reported with positively charged peptides[43] and proteins.[44] P23 binding has the same profile as P2 binding (Figure 3C).

The changes in the aspect ratios from the UV/Vis spectra as the peptide concentration increased were also monitored. The gradual shift of the absorption band in Figure 3B and C around 630 nm indicates the formation of AuNP dimers, perhaps trimers. The aspect ratio can be approximated using the formula λmax = 96AR + 418.[45] This formula generates AuNPs with an approximate aspect ratio of 1.06, which is consistent with the expected aspect ratio of our citrate reduced AuNPs used in this study. When the absorbance band forming at around 620 nm is considered (Figures 3B and 3C), the aspect ratio reached 2.10 and this value slightly increased with increased peptide concentration. Although this information is important and apparent, it does not provide further information about the aggregation status of the AuNPs in a suspension.

On the binding of P23 to the AuNP surface a 5–6-nm red shift occurred. The SPR red shift of P23 is larger than that of P2 because of the net charge of P2 (+2.0) and P23 (+16.8) at pH 6. P23 may be stacked at the AuNP surface and this stacking causes the big red shift. It is clear that the degree of the red shift depends on the chemical structure and size of the positively charged peptide. The other interesting observation is the intensity change of the emerging band at around 650 nm. The maximal intensity of the emerging band does not exceed the maximal intensity of the SPR band with larger peptides (P23), while an exceeding intensity was

observed with shorter peptides (P2). This may indicate that more AuNP peptide aggregates are formed in the suspension when shorter peptides are used. We used water instead of peptide for the control experiments, which caused a slight decrease in the SPR band, possibly the effect of dilution. There was no shift in the position of the SPR band in the control experiments. Our results showed that up to a 350 times higher concentration of P23 the SPR band decreased linearly ($R^2 = 0.998$). Furthermore, P23 bound tightly to AuNPs via ionic interactions (Figure 3D).

When the DLS data (Figures 4A and 4B) are considered, the size of the AuNP aggregates becomes much larger (up to 150 nm) than the aspect ratio indicated size from the UV/Vis data. With the SAXS measurements, we aimed to take a deeper look into how the AuNP aggregates are formed in the liquid phase.

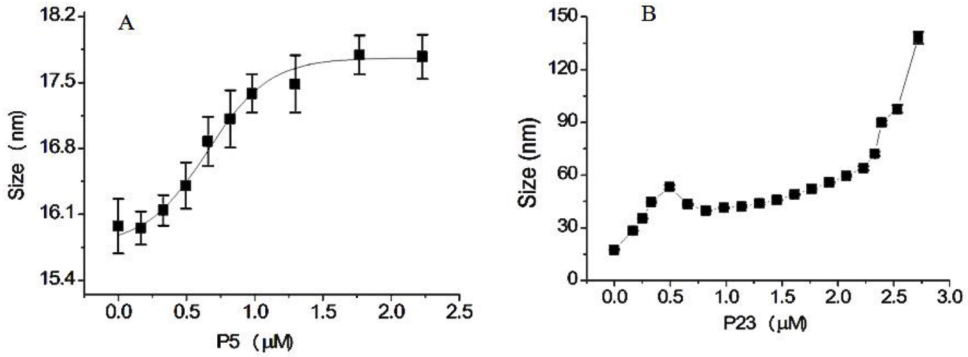

Figure 4. The size distribution pattern of the AuNPs with the addition of the negatively charged peptide P5 (A). The measured DLS profile of the P5 binding fits a sigmoidal function. The size distribution pattern of the AuNPs with the addition of the positively charged peptide P23 (B).

The size distribution analysis of P5 titrations was performed with DLS. It is known that the surface of AuNPs is covered with a citrate layer and the hydrodynamic diameter of the AuNPs is measured by DLS. Our results indicated that the surface citrate is replaced by P5 with each addition of it. According to the DLS measurements, the size distribution of AuNPs–P5 increases with the addition of P5 peptide. All surfaces of AuNPs will be covered by P5 at the saturated P5 concentration.

2.4. Small-angle X-ray scattering (SAXS) study

It is critical to understand the behavior of NPs in suspension and relate this information to their assembly on surfaces. Small-angle X-ray scattering (SAXS) is a principal technique for structure analysis of materials and nanocomposites.[46] Therefore, the behavior of systematically modified AuNPs in suspension was investigated. As mentioned before, we had clues that the positively charged peptide-coated AuNPs formed a network in suspension depending on the peptide length and charge. The SAXS spectra of the AuNP are presented in Figure 5A. All the spectra overlap well on a large range and display distinctive maxima, characteristic of spherical NPs. Differences can be seen in the initial part of the SAXS spectrum very sensitive to interparticle interactions: while (i) the scattering from the negatively charged NPs does not vary in function of the peptide attached to the surface and stays close to blank AuNPs, (ii) the AuNPs coated with positively charged peptides differ significantly from the blank AuNPs. This indicates that the structures of AuNPs in the different samples are similar, but their interactions in solution are different.

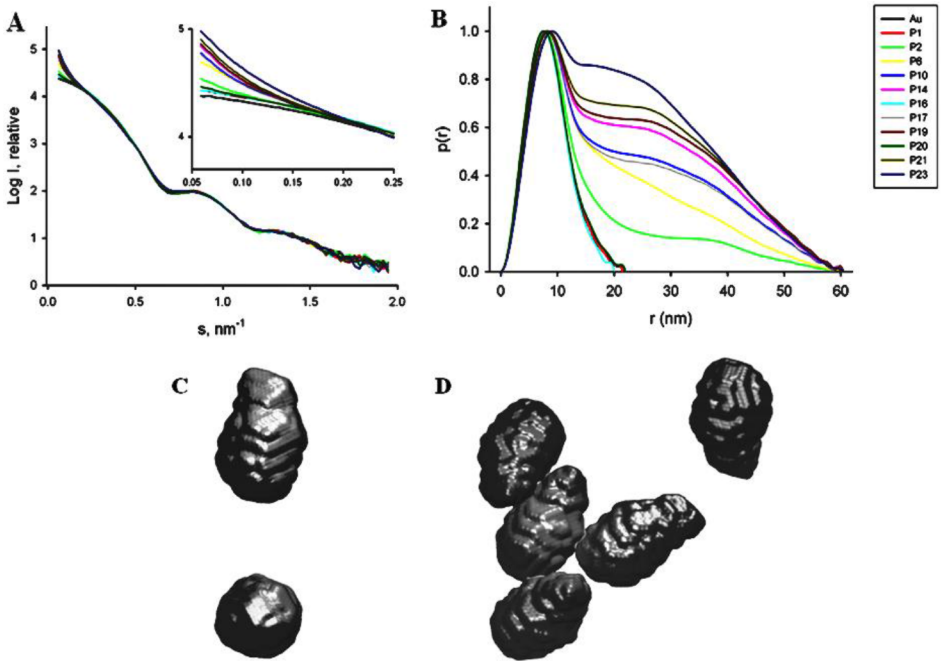

Figure 5. Small-angle X-ray scattering analysis of the AuNPs positively and negatively charged peptides (A). Distance distribution functions (B). Modeled structures of an AuNP (C) and P23 modified AuNPs (D) in suspension in the form of a network as obtained from the SAXS experiment using DAMMIF.

The radius of gyration of the individual NPs was estimated by calculating the distance distribution function on a truncated spectrum. The initial part ($s < 0.45$ nm^{-1}) was not considered here and so the interaction between the NP can be disregarded. The Rg values of the different samples agree well with each other within the experimental error and are between 5.35 and 5.7. The radius of a homogeneous sphere is calculated from the radius of gyration using the following equation: $(R_{single})^2 = (3/5)R^2$. The Rg found leads to a radius between 6.9 and 7.3, which is slightly larger than the expected radius of 6.5 nm.

The distance distribution functions were also calculated using the initial portion of the curves and are represented in Figure 5B after re-normalization. This permits us to underline the differences between negatively and positively charged NPs. For negatively charged and pure NPs, the distance distribution function is close to a Gaussian center around 7.5, somehow larger than what is expected for 13 nm NPs, but consistent with the Rg previously computed. For positively charged NPs, longer distances are present in addition to this Gaussian. Moreover, the proportion of long distance in this distance distribution increases with the length of the peptide bound to the NPs. The Rg of the cluster was also determined using this distance distribution function.

By supposing a similarity in shape of the cluster and the individual NPs, one can roughly estimate the number of monomers in the cluster from the radius of gyration of the cluster and individual NPs: $n = (Rg/R_{single})^3$. The Rg and n values are reported in Table 2. They underline the difference between negatively and positively charged AuNPs: the n computed for a negatively charged value is rather small (around 2); it is consistent with the absence of the large structure already seen in the distance distribution function. For positively charged AuNPs, n is much higher and increases with the length of the peptide, around 20 for the short peptide; it goes up to 80 for the longest peptides.

Table 2. Shape similarity of the cluster and the individual NP.

Filename	Ragg	RgNP	N
Au	6.79	5.58	1.8
P1	6.78	5.55	1.8
P2	14.3	5.55	17.1
P6	16.85	5.46	29.4
P10	20.22	5.44	51.4
P14	20.13	5.42	51.2
P16	6.86	5.57	1.9
P17	22.43	5.43	70.5
P19	22.72	5.39	74.9
P20	7.3	5.55	2.3
P21	23.56	5.38	84
P23	22.51	5.37	73.7

The SAXS data were further used to build models in 2 steps: firstly, the blank and negatively charged AuNPs, showing no sign of aggregation, were used to build models of single NPs; in the second step, the model obtained for individual NPs was used to model the aggregates seen for positively charged AuNPs. The dummy atom model of single NPs was built using the program DAMMIF. The models obtained for the blank AuNPs and the negatively charged peptide coated AuNPs are very similar. This was to be expected given the similarity in the SAXS pattern and distance distribution. The model obtained for the blank AuNPs is shown in Figure 5C. It has a prolate spheroid shape with a semimajor axis close to 10 nm and a semiminor axis close to 6 nm. Due to its low electronic density compared to the AuNPs, the peptide layer is not seen by SAXS. This could already be inferred from the similarity in the SAXS patterns and distance distribution functions of blank and negatively charged AuNPs. It allows us to use the model of individual NPs previously obtained for the blank AuNPs as an elemental building block for the rigid body modeling of aggregates.

The interaction between NPs can be seen for positively charged AuNPs in the initial part of the SAXS curve. This part is then used to model the aggregates with a rigid body approach. Due to its low electronic density compared to AuNPs, the peptide layer is not seen by SAXS. This could already be inferred from the similarity in the SAXS patterns and distance distribution functions of blank and negatively charged AuNPs. It allows one to use the model of individual NPs previously obtained for the blank AuNPs as an elemental building block for the rigid body modeling of aggregates.

The rigid body approach was performed using the minimum amount of AuNPs sufficient to fit the experimental data. A typical rigid body model is obtained on the AuNPs is represented in Figure 5C by fitting to the experimental data. In this model, 2 AuNPs were necessary to obtain a good fit to the experimental data. In the case of the AuNPs–P23 model, 5 AuNPs were necessary to obtain a good fit (Figure 5D).

2.5. AFM study

Finally, attempts were made to transfer the AuNP–peptide structures onto surfaces to examine with AFM. The data presented in Figures 6A–6D were acquired from 20 $\times$ 20 μm or 40 $\times$ 40 μm areas. As seen, there is almost no pattern difference between the dried droplet areas of the citrate capped (Figure 6A) and negatively charged peptide (P20) modified AuNPs and aggregates are distributed on the mica surface randomly (Figure 6B). Due to the high density of negative charges, the negatively charged peptide coated AuNPs cannot form networks or larger aggregates. A major player during the drying of a droplet is the "coffee-ring phenomenon", which drags

all molecular species and colloidal particles freely wandering in the suspension to the droplet edges.[47] The lack of attractive forces between the modified AuNPs and its aggregates cannot defy the dragging forces in a droplet. In the case of the positively charged peptide modified AuNPs, the formation of linear and branched wire-like structures within a compact network on the droplet area was observed from AFM images as seen in Figures 6C and 6D. This is possibly due to the formation of bridges between the AuNPs and their smaller aggregates through the peptides chemically attached to the AuNPs.[16]

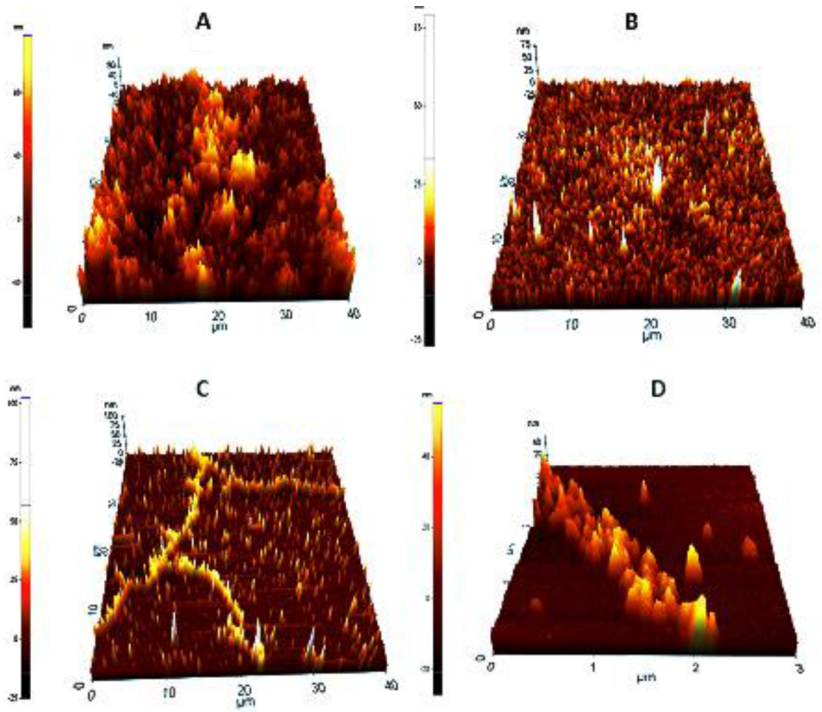

Figure 6. AFM images of the peptide modified AuNPs. AuNPs (A), P20 modified AuNPs (B), P23 modified AuNPs. Wire-like assembled AuNPs packaged with P23 (C), taking a closer look at AuNPs–P23 assembly (D).

The sizes of the formed extended structures become greater with the increase in positive charge and size of peptide. When the structures are examined more closely with AFM by scanning 3 × 3 μm area (Figure 6D), it can be seen that the width of the wire-like structure is nearly 500 nm and it has a height of 1 or 2 AuNPs. This indicates that the structures formed are a few NPs thick and 35–40 NPs wide flat structures. The formation of such extended networks on surfaces also indicates that when the NPs are interconnected, they can escape from getting jammed at the liquid–solid–air contact line partially if not wholly.

3. Experiment

3.1. Materials

$HAuCl_4 \cdot 3H_2O$ (Puriss p.a. ACS; ≥49% Au) was purchased from Sigma-Aldrich. Sodium citrate (99%–101%) was bought from Merck (Darmstadt, Germany). CaF_2 polished glass slides 70 × 26 × 1 mm were purchased from Crystran Ltd (UK). Mika and noncontact silicon nitrile tips were purchased from Electron Microscopy Science and Park Systems, respectively. To prepare all solutions, deionized and autoclaved water (Direct-Q_{uv} Element, Millipore) were used. The designed peptides were synthesized by CPC Scientific, Inc.

(Sunnyvale, CA, USA) and provided in lyophilized form. Stock solutions of all the peptides were prepared as 10^{-3} M and stored at –20 °C until used.

3.2. Preparation of AuNPs

The AuNPs were prepared by reduction of $HAuCl_4 \cdot 3H_2O$ with sodium citrate. This procedure generates an average size of about 15 nm AuNPs that are well characterized in the literature.[48] Briefly, 50 mL of 38.8 mM citrate stock solution was added to 500 mL of 1 mM $HAuCl_4 \cdot 3H_2O$ solution. The $HAuCl_4 \cdot 3H_2O$ solution was heated until it boiled, and then the citrate solution was added to the boiling solution. The final solution was kept at the same temperature for 15 min. Optical absorption spectra of AuNP suspension were registered on a double-beam UV/VIS spectrophotometer Lambda 35 (PerkinElmer, Germany) by scanning in the range of 300–900 nm at room temperature. The concentration of AuNPs synthesized by citrate reduction was calculated using the of extinction coefficient and the averaged size.[38]

3.3. Peptide-binding studies

The peptide binding experiments were conducted by titrating AuNP suspensions against 50 μM peptide stock solution in a polystyrene cuvette and by recording the changes in the plasmon absorption spectrum of the AuNPs. The titration was performed by adding 5 μL stepwise into 3 mL of AuNP suspension. All experiments were performed at an ambient temperature.

3.4. Size and zeta potential measurements

The size distribution and zeta potential measurements of the NPs were performed with a Zetasizer Nano ZS (Malvern, USA) at 25 °C. The Nano ZS contains a 4-mW He–Ne laser operating at a wavelength of 633 nm and an avalanche photodiode detector. The scattered light was detected at an angle of 173°. The refractive index and absorption of the colloidal suspension were assumed to be 2.0 and 0.320, respectively. All size and zeta potential measurements were carried out in triplicate. All data were analyzed by using the Malvern instrument DST 5.00 software.

3.5. SERS measurements

All SERS measurements were performed using a completely automated Renishaw InVia Reflex Raman microscopy system (Renishaw Plc., New Mills, Wotton-under-Edge, UK) equipped with an 830 nm diode laser. The laser power was 30 mW and the exposure time was 10 s. A 20× objective was used. The wavelength of the instrument was automatically calibrated using an internal silicon wafer, and the spectrum was centered at 520 cm^{-1}. All spectra were taken with the 830 nm wavelength laser. Next, 2 μL of AuNP-peptide suspension was spotted on a CaF_2 slide, which gives nearly zero background spectra, and the spectra obtained from each suspension were evaluated.

3.6. SAXS studies

The synchrotron radiation X-ray scattering data from solutions of peptide modified AuNPs were collected on the X33 camera of the EMBL on the storage ring DORIS III (DESY, Hamburg, Germany).[49] Using a Pilatus 1M-W image plate detector at a sample-detector distance of 2.7 m and a wavelength of $\lambda = 1.5$ Å, the range of momentum transfer $0.01 < s < 0.6$ $Å^{-1}$ was covered ($s = 4\pi \sin\theta/\lambda$, where 2θ is the scattering angle). For each construct, 8 successive 15-s exposures were collected. The data were normalized to the intensity of

the transmitted beam and radially averaged; the scattering of the buffer was subtracted and the difference curves were scaled for NP concentration. The data processing steps were performed using the program package PRIMUS.[50] The pair distance distribution function was calculated using the program GNOM.[51]

The SAXS curves were further used to generate the low resolution ab initio shapes of individual NPs by the program DAMMIF.[52] This program represents the particle shape by an assembly of densely packed beads and employs simulated annealing to construct a compact interconnected model fitting the experimental data $I_{exp}(s)$ to minimize discrepancy.

$$\chi^2 = \frac{1}{N-1}\sum_j \left[\frac{I_{exp}(s_j) - cI_{calc}(s_j)}{\sigma(s_j)}\right]^2 \quad (1)$$

where N is the number of experimental points, c is a scaling factor, and $I_{calc}(s)$ and $\sigma(s_j)$ are the calculated intensity and the experimental error at the momentum transfer sj, respectively. Rigid body refinement of the structure of the cluster was performed using the program SASREF.[53] Starting from the tentative model, this program uses simulated annealing to search for a nonoverlapping interconnected configuration of domains fitting the experimental data.

3.7. AFM studies

A Park Systems XE 100 Atomic Force Microscope (Park Systems Corp., Korea) was used for imaging at ambient temperature. The samples were prepared as described above and were spotted on freshly cleaved mica and dried at room temperature. Noncontact silicon nitrile tips with varying resonance frequencies were used in the analyses. The scan rate was 0.5 Hz. The surface roughness measurements were performed by locating the cursor line on 10 different locations with 0.5-μm steps on the AFM images. The 10 roughness values indicated by the software were averaged.

4. Conclusion

In this study, we aimed to understand the behavior of peptide coated AuNPs in suspensions and at the liquid–solid interface. SERS was used to verify the chemical attachment of peptides onto the AuNP surfaces. As AuNPs were modified with anionic peptides, no significant change in their behavior in suspension was observed. A slight intensity increase from 520 nm to 523 nm of the maximum absorption peak on UV/Vis spectra was observed with increasing concentration of anionic peptide. From the DLS measurements, small changes in hydrodynamic size and zeta potential were observed. As the cationic peptides are used to coat the AuNP surfaces, size and charge dependent aggregation of AuNPs are observed. Increasing peptide size and cationic charge results in larger aggregates as confirmed by DLS and SAXS experiments. The DLS data show that the size of the aggregates can be as large as 150 nm but the SAXS evaluations indicate up to 80 nm. The difference in these 2 techniques could result from the nature of the techniques. However, one clear conclusion is that the aggregate size gets larger with the size and the number of charges on the peptide. Although the "coffee-ring phenomenon" is the major player during the drying of a suspension droplet left on a surface, the dried droplet area can provide valuable information on the status of the colloidal particles in a droplet of the suspension. The AFM images of the dried droplet areas indicate the formation of linear and branched networks of positively charged peptide coated AuNPs and their aggregates. The combined data from UV/Vis, DLS, and AFM SAXS experiments suggest that the positively charged peptides form network-like linear structures in the suspension as their size gets larger. A number of indicators such as failure to obtaini zeta potential from

the larger positively charged peptide coated AuNPs and resisting dragging forces exerted by the "coffee-ring phenomenon" as confirmed by AFM study also suggest the formation of 3D network-like structures in the suspension. In conclusion, it was found that charge and size of the peptides have a dominating effect on the assembly of peptide modified AuNPs and they can be utilized to influence the behavior of NPs for manipulation to bring them to higher structures.

Acknowledgments

The authors gratefully acknowledge the financial support from TÜBİTAK (grant no: 108T605) and Yeditepe University during this study. The authors also gratefully acknowledge Deutsches Elektronen - Synchrotron (DESY) (Hamburg, Germany) for allowing the use of their facilities for performing the SAXS experiments.

References

1. Chung, S. W.; Ginger, D. S.; Morales, M. W.; Zhang, Z. F.; Chandrasekhar, V.; Ratner, M. A.; Mirkin, C. A. *Small* **2005**, *1*, 64–69.
2. Liu, S. T.; Maoz, R.; Sagiv, J. *Nano Lett.* **2004**, *4*, 845–851.
3. Fendler, J. *Chem. Mater.* **2001**, *13*, 3196–3210.
4. Whitesides, G. M.; Boncheva, M. *PNAS* **2002**, *99*, 4769–4774.
5. Loweth, C. J.; Caldwell, W. B.; Peng, X. G.; Alivisatos, A. P.; Schultz, P. G. *Angew. Chem. Int. Edit.* **1999**, *38*, 1808–1812.
6. Coomber, D.; Bartczak, D.; Gerrard, S. R.; Tyas, S.; Kanaras, A. G.; Stulz, E. *Langmuir* **2010**, *26*, 13760–13762.
7. Seela, F.; Budow, S. *Nucleosides Nucleic Acids* **2007**, *26*, 755–759.
8. Teixido, M.; Giralt, E. *J. Pept. Sci.* **2007**, *14*, 163–73.
9. Yuan, B.; Xing, L.; Zhang, Y. D.; Lu, Y.; Mai, Z. H.; Li, M. *J. Am. Chem. Soc.* **2007**, *129*, 11332–11333.
10. Jeong, H. S.; Kyouichi, A.; Bong, K. L.; Dong, G. K.; Yeon, K. K.; Kyoung, R. K.; Hea, Y. L.; Tomoji, K.; Hyung, J. C. *Bioconjugate Chem.* **2007**, *18*, 2197–2201.
11. Aili, D.; Enander, K.; Rydberg, J.; Nesterenko, I.; Björefors, F.; Baltzer, L.; Liedberg, B. *J. Am. Chem. Soc.* **2008**, *130*, 5780–5788.
12. Si, S.; Mandal, T. K. *Langmuir* **2007**, *23*, 190–195.
13. Ding, Y.; Xia, X. H.; Zhai, H. S. *Chemistry* **2007**, *13*, 4197–4202.
14. Mankar, S.; Anoop, A.; Sen, S.; Maji, S. K. *Nano Reviews* **2011**, *2*, 6032–6044.
15. Basu, S.; Ghosh, S. K.; Kundu, S.; Panigrahi, S.; Pande, S.; Jana, S.; Pal, T. *J. Colloid Interface Sci.* **2007**, *313*, 724–734.
16. Tullman, J. A.; Finney, W. F.; Lin, Y. J.; Bishnoi, S. W. *Plasmonics* **2007**, *2*, 119–127.
17. Levy, R.; Thanh, N. T.; Doty, R. C.; Hussain, I.; Nichols, R. J.; Schiffrin, D. J.; Brust, M.; Fernig, D.G. *J. Am. Chem. Soc.* **2004**, *126*, 10076–10084.
18. Chen, C. L.; Zhang, P. J.; Rosi, N. L. *J. Am. Chem. Soc.* **2008**, *130*, 13555–13557.
19. Krpetic, Z.; Nativo, P.; Porta, F.; Brust, M. A. *Bioconjugate Chem.* **2009**, *20*, 619–624.
20. Rand, D.; Ortiz, V.; Liu, Y.; Derdak, Z.; Wands, J. R.; Taticek, M.; Petruck, C. R. *Nano Lett.* **2011**, *11*, 2678–2683.
21. Derjaguin, B.; Landau, L. *Acta Physico Chemica* **1941**, *14*, 633–662.
22. Lin, S. Y.; Tsai, Y. T.; Chen, C. C.; Lin, C. M.; Chen, C. H. *J. Phys. Chem. B* **2004**, *108*, 2134–2139.
23. Serizawa, T.; Hirai, Y.; Aizawa, M. *Langmuir* **2009**, *25*, 12229–12234.

24. Feigin, L. A.; Svergun, D. I. *Structure Analysis by Small-Angle X-Ray and Neutron Scattering*; Plenum Press: New York, NY, USA, 1987.
25. Shtykova, E. V.; Malyutin, A.; Dyke, J.; Stein, B.; Konarev, P. V.; Dragnea, B.; Svergun, D. I.; Bronstein, L. M. *J. Phys. Chem. C* **2010**, *114*, 21908–21913.
26. Medina, S. D.; McDonough, S.; Swanglap, P.; Landes, C. F.; Link, S. *Langmuir* **2012**, *19*, 9131–9139.
27. Lopez, S. G.; Juarez, J.; Meda, M. A.; Casals, E.; Puntes, V. F.; Taboada, P.; Mosquera, V. *Langmuir* **2012**, *28*, 9113–9126.
28. Westcott, S. L.; Oldenburg, S. J.; Lee, T. R.; Halas, N. J. *Langmuir* **1998**, *14*, 5396–5401.
29. De, M.; Ghosh, P. S.; Rotello, V. M. *Biology Adv. Mater.* **2008**, *20*, 4225–4241.
30. Tsen, M.; Sun, L. *Anal. Chim. Acta.* **1995**, *307*, 333–340.
31. Oyelere, A. K.; Chen, P. C.; Huang, X.; El-Sayed, I. H.; El-Sayed, M. A. *Bioconjugate Chem.* **2007**, *18*, 1490–1497.
32. Maiti, C. N.; Apetri, M. M.; Zagorski, M. G.; Carey, P. R.; Anderson, V. E. *J. Am. Chem. Soc.* **2004**, *126*, 2399–408.
33. Gearheart, L. A.; Ploehn, H. J.; Murphy, C. J. *J. Phys. Chem. B* **2001**, *105*, 12609–12615.
34. Movasaghi, Z.; Rehman, S.; Rehman, I. U. *Applied Spectroscopy Reviews* **2007**, *42*, 493–541.
35. Stewart, S.; Fredericks, P. M. *Spectrochimica Acta Part A* **1999**, *55*, 1615–1640.
36. Graf, P.; Mantion, A.; Foelske, A.; Shkilnyy, A.; Masic, A.; Thunemann, A. E.; Taubert, A. *Chem. Eur. J.* **2009**, *15*, 5831–5844.
37. Garrido, C.; Aliaga, A. E.; Jeria, J. S. J.; Clavijo, R. E.; Vallette, M. M. C.; Cortes, S. S. *Journal of Raman Spectroscopy* **2010**, *41*, 1149–1155.
38. Horovitz, O.; Mocanu, A.; Tomoaia, G.; Bobos, L.; Dubert, D.; Daian, I.; Yusanis, T.; Cotisel, M. T. *Stud. Univ. Babes. Bolyai. Chem.* **2007**, *52*, 97–108.
39. Sellers, H.; Ulman, A.; Shnidman, Y.; Eilers, J. E. *J. Am. Chem. Soc.* **1993**, *115*, 9389–9401.
40. Creighton, J. A.; Eadon, D. G. *J. Chem. Soc., Faraday Trans.* **1991**, *87*, 3881–3891.
41. Liu, X.; Atwater, M.; Wang, J.; Huo, Q. *Colloids and Surfaces B: Biointerfaces* **2007**, *58*, 3–7.
42. Haiss, W.; Thanh, N. T.; Aveyard, J.; Fernig, D. G. *Anal. Chem.* **2007**, *79*, 4215–4221.
43. Savage, A. C.; Pikramenou, Z. *Chem. Commun.* **2011**, *47*, 6431–6433.
44. Juan, S. X.; Dan, L.; Jing, X.; Shawn, W.; Qiang, W. Z.; Hong, C. *Chin. Sci. Bull.* **2012**, *57*, 1109–1115.
45. Brioude, A.; Jiang, X. C.; Pileni, M. P. *J. Phys. Chem. B* **2005**, *109*, 13138–13142.
46. Fratzl, P. *J. Appl. Cryst.* **2003**, *36*, 397–404.
47. Maki, K. L.; Kumar, S. *Langmuir* **2011**, *27*, 11347–11363.
48. Lee, P. C.; Meisel, D. *J. Phys. Chem* **1982**, *86*, 3391–3395.
49. Blanchet, C. E.; Zozulya, A. V.; Kikhney, A. G.; Franke, D.; Konarev, P. V.; Shang, W.; Klaering, R.; Robrahn, B.; Hermes, C.; Cipriani, F.; et al. *J. Appl. Cryst.* **2012**, *45*, 489–495.
50. Konarev, P. V.; Volkov, V. V.; Sokolova, A. V.; Koch, M. H. J.; Svergun, D. I. *J. Appl. Cryst.* **2003**, *36*, 1277–1282.
51. Svergun, D. I. *J. Appl. Cryst.* **1992**, *25*, 495–503.
52. Franke, D.; Svergun, D. I. *J. Appl. Cryst.* **2009**, *42*, 342–346.
53. Petoukhov, M. V.; Svergun, D. I. *Biophys. J.* **2005**, *89*, 1237–1250.